




 Cite this: *Nanoscale*, 2021, **13**, 9825

Surface ligand rigidity modulates lipid raft affinity of ultra-small hydrophobic nanoparticles: insights from molecular dynamics simulations†

 Xiaoqian Lin ^{a,b} and Xubo Lin ^{*a}

Differential preferences between lipids and proteins drive the formation of dynamical nanoscale membrane domains (lipid rafts), which play key roles in the proper functioning of cells. On the other hand, due to the potent physicochemical properties of nanoparticles (NPs), they have been widely used in drug delivery, bio-imaging and regulating various essential biological processes of the cells. Hence, in this work, we aim to design ultra-small hydrophobic NPs with tunable raft affinity, which is supposed to partition into the hydrophobic region of lipid membranes and be able to regulate the dynamics of the lipid raft domains. A series of μ s-scale coarse-grained molecular dynamics simulations and umbrella sampling free energy calculations were performed to investigate the role of surface ligand rigidity of ultra-small hydrophobic NPs in their raft affinity. Our results indicated that the preferred localization of NPs can be tuned by adjusting their surface ligand rigidity. Generally, rigid NPs tended to target the raft domain, while soft NPs preferred the interface of the raft and non-raft domains. The free energy analysis further indicated that the surface ligand rigidity of NPs can enhance their targeting to lipid raft domains. Besides, we found that these ultra-small NPs had no significant effects on the phase separation of the lipid membrane although they might cause some local interference to surrounding lipids. These results indicate that the targeting to the lipid raft domain can be achieved by the surface ligand rigidity of NPs, which provides helpful insights for further regulations of lipid raft-mediated biological processes.

Received 11th March 2021

Accepted 3rd May 2021

DOI: 10.1039/d1nr01563j

rsc.li/nanoscale

Introduction

In the past several decades, nanoparticles (NPs) have been widely used in many biomedical applications such as bio-imaging,^{1,2} drug carriers^{3–7} and implant materials.⁸ In order to further broaden the biomedical applications of NPs, it is very essential to study the interactions between NPs and cells, which serve as the basic structural and functional units of organisms. As the first selection barrier of cells, the cell membrane consists of various lipids and proteins, which participate in many important biological processes. Hence, understanding the interactions of NPs with cell membranes in detail is of great importance for their potential biomedical applications.^{5,9,10} As indicated by both experimental and computational research studies, penetration mechanisms of NPs

across the cell membrane vary with their physicochemical properties including size,^{11,12} shape,^{13–15} or surface properties.^{5,16} In particular, ultra-small hydrophobic NPs can penetrate into the hydrophobic region of the cell membrane.^{17,18} It has been shown that the preferred localization of these hydrophobic NPs can be regulated by the hydrophobicity, grafting density and charge of the surface ligands.^{19–21} In addition, ligand rigidity has been shown to be important in NPs' translocation processes across the cell membrane.^{22–25} However, it is still not clear whether the surface ligand rigidity can affect NPs' preferred localization in the cell membrane.

In the cell membrane, thousands of lipids and proteins work together to achieve their critical biological functions. Due to the differential interaction preferences between these molecules, the cell membrane can segregate into a series of nanoscale dynamical and ordered membrane domains (lipid rafts).^{26,27} Generally, the dynamics of lipid rafts, which includes both the inner-leaflet and inter-leaflet dynamics, can be modulated by lipid/protein compositions, interleaflet coupling strength and embedded nanoparticles.^{28–33} The inner-leaflet dynamics of the raft domain is mainly regulated by the differences in the lipid chain unsaturation,²⁸ which can further affect the partitioning thermodynamics of the trans-

^aInstitute of Single Cell Engineering, Key Laboratory of Ministry of Education for Biomechanics and Mechanobiology, Beijing Advanced Innovation Center for Biomedical Engineering, School of Biological Science and Medical Engineering, Beihang University, Beijing 100191, China. E-mail: linxbseu@buaa.edu.cn

^bShen Yuan Honors College, Beihang University, Beijing 100191, China

† Electronic supplementary information (ESI) available: Additional figures. See DOI: 10.1039/d1nr01563j

membrane proteins.^{30,33} Factors such as the lipid acyl chain *cis* double bond position³¹ and the cholesterol flip-flop rate³² could affect the interleaflet coupling strength and thus modulate the interleaflet dynamics of the raft domain. The disruption of lipid raft domain stability and dynamics may be closely related to many diseases including infectious diseases, cardiovascular diseases, and tumors.^{34–37} Hence, it is important to design NPs with appropriate surface properties to target either the lipid raft or non-raft domains. NPs with specific raft affinity may regulate not only the lipid raft domain stability and dynamics, but also protein dynamics within the membrane domains. In this work, we will reveal the correlation between the surface ligand rigidity of NPs and their affinity to lipid raft domains.

In order to achieve the above goal, molecular dynamics (MD) simulation, which is widely used to quantify the interactions between NPs and lipid membranes at the molecular/atomic scales,^{38–42} may provide a powerful computational tool for the purpose. In particular, coarse-grained (CG) MD simulations make it more feasible to study the lipid raft membrane systems,^{20,43–47} which requires a length scale of tens of nm and a time scale of a few μ s. For example, Lunnoo *et al.*⁴³ revealed the internalization pathways of Au nanostructures with different sizes, shapes, surface charges, and aggregation states across mammalian model plasma membranes *via* CGMD simulations. Liang *et al.*²⁰ used CGMD simulations to study the interactions between NPs coated with neutral/charged ligands and phase-separated lipid bilayers. They proposed that the penetration and adsorption process of NPs and the final distribution can be easily modulated by changing the ligand density and the surface charge of NPs. On the other hand, many experiments have indicated that ultra-small hydrophobic NPs can be easily encapsulated into the hydrophobic region of the lipid membrane.^{18,48} In the current work, we will employ μ s-scale CGMD simulations to reveal the correlations between the surface ligand rigidity of hydrophobic NPs and their raft affinity. Umbrella sampling simulations as well as the weighted histogram analysis method (WHAM)⁴⁹ are used to obtain the penetration free energy of these NPs from the bulk water region to the interior of lipid membranes.

Model and methods

Molecular dynamics simulation

CGMD simulations have been widely used to study proteins and lipid membranes. In the current study, we used the MARTINI CG model⁴⁷ (version 2.0) and the GROMACS simulation package⁵⁰ (version 2016.05) to study the dynamical behavior of the lipid raft membrane systems. The Martini CG model is based on a four-to-one mapping, *i.e.*, on average four heavy atoms are represented by a single interaction center, which includes four main types of CG beads: polar (P), apolar (C), non-polar (N) and charged (Q), and each bead type can be further divided into 4 or 5 different levels, a total of 20 subtypes, which can more accurately represent the chemical pro-

erties of the basic atomic structure. All CGMD simulations in this work were run with constant pressure and temperature, as well as periodic boundary conditions. The temperature was controlled by v-rescale heat baths⁵¹ at $T = 310$ K with $\tau = 1$ ps for lipids and water plus ions. The pressure was kept at 1 bar using a semi-isotropic Parrinello–Rahman pressure coupling scheme⁵² with a coupling constant $\tau = 5$ ps and a compressibility of 3×10^{-4} per bar. The default value of the relative dielectric constant of the force field was 15. The particle-mesh Ewald method with a real-space cutoff of 1.2 nm was used to calculate the electrostatic interactions, which was smoothly shifted to zero from 0 to 1.2 nm. The Lennard-Jones potential was smoothly shifted to zero between 0.9 and 1.2 nm, with a cutoff of 1.2 nm to reduce the cutoff noise. Generally, each CGMD simulation was run for 5 μ s (effective time was around 20 μ s) with a time step of 20 fs and a trajectory-saving frequency of 500 ps.

Nanoparticles

In the current study, we constructed a smooth surface NP core by uniformly distributing Martini CG beads on a concentric spherical surface with a basic packing constant of 0.47 nm. The core diameter is about 2.2 nm and consists of 59 CG beads, of which C5 type CG beads are used to mimic the hydrophobic NP core similar to the gold NP.⁵³ As for the surface ligands of NPs, inspired by previous work,²¹ we used 5 C1 type CG beads for them (Fig. 1a), which have the potential to target lipid raft domains. The equilibrium distance between two adjacent beads is 0.47 nm, and the ligand is uniformly modified on the surface of the NP core. The surface ligand rigidity is adjusted by changing the force constant of the bond angle constraints within the ligand, which is adapted from previous dissipative particle dynamics simulations.²⁵ On the one hand, the simplified treatment enables us to study the exact role of the ligand rigidity (the only variable) in physics-based simulations. On the other hand, it can directly represent the case that changes in the ligand rigidity are caused by changes in the ligand physical structures (*e.g.* temperature-sensitive polymers⁵⁴).

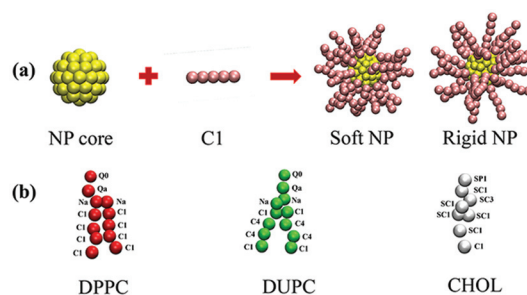


Fig. 1 Schematic illustrations of the coarse-grained lipids and NPs used in this work. (a) Ligand-modified NPs with different ligand rigidities. An NP core is colored in yellow and the ligand in pink. (b) Saturated lipids (DPPC), unsaturated lipids (DUPC) and cholesterol (CHOL). DPPC is colored in red, DUPC in green, and CHOL in white. All the snapshots in this work are generated by VMD.⁵⁵

Lipid bilayers

The initial symmetric bilayers were set up with the tool *insane.py* developed by Wassenaar *et al.*⁵⁶ We chose the widely used three-component lipid bilayer containing saturated dipalmitoyl-phosphatidylcholine (DPPC), unsaturated dilinoleoyl-phosphatidylcholine (DUPC), and cholesterol (CHOL) molecules in a molar ratio of 5 : 3 : 2.^{28,57} The MARTINI-based configurations of DPPC, DUPC and CHOL molecules can be found in Fig. 1b. Among them, a DPPC/DUPC molecule is composed of 12 CG beads. The headgroup consists of two charged beads and two nonpolar beads forming the glycerol ester backbone (GLY). Each of the two tails includes four apolar beads (C1/C4). A CHOL molecule is composed of 8 CG beads. Here, each system includes 572 DPPC, 342 DUPC, 228 CHOL, 21873 water molecules and 0.15 M NaCl. The initial box size is 20 nm × 20 nm × 10 nm. After energy minimization, each system was simulated at $T = 400$ K and the isobaric isothermal (NPT) ensemble to homogenize the distribution of molecules for the reasonable initial system configuration. Then, the system was gradually adjusted to the body temperature ($T = 310$ K) and went through the production run of 5 μ s. In the initial 1 μ s CGMD simulation, the lipid membrane showed a clear phase separation, which allowed us to quantify the partitioning dynamics of NPs in phase-separated lipid membranes during the subsequent 4 μ s simulation period.

Analysis of trajectories

Two-dimensional (2D) number-density map. To explore the localization of NPs in the lipid membrane, the two-dimensional number density map of DPPC molecules and the movement tracking of NPs were carried out. Here, the motion of the NP was recorded, in which the black points represented the position of the center-of-mass (COM) of the NP during the last 1 μ s trajectory. Meanwhile, the GROMACS tool *gmx densmap* was used to generate the 2D number density map of the DPPC molecules. All DPPC COM positions in the last 1 μ s trajectory can be mapped to the x - y plane of the lipid membrane. The number density was calculated based on these points on the 2D plane, and all points were colored according to their number density for visualization. In the 2D density map, the high probability area represents the lipid raft domain, while the low probability area represents the lipid non-raft domain. By simply superimposing the two analysis data, we can determine the relative partition preferences of NPs of different stiffnesses.

NP's preference for lipid rafts or non-rafts. In order to reveal the effects of surface physicochemical properties of NPs on their preferred localization, NP's preference to lipid rafts or non-rafts can be determined directly based on the number of contacts of NPs with raft lipids (DPPC and CHOL) and non-raft lipids (DUPC) using the GROMACS tool *gmx mindist* (cutoff: 0.6 nm).

Lipid chain order parameters. The lipid chain order parameter (S_z) can be calculated using the formula

$$S_{z,n} = \frac{1}{2} (3 \cos^2 \theta_n - 1)$$

where θ_n is the angle between the vector connecting the $n - 1$ and $n + 1$ beads of the lipid tail and the bilayer normal z , and the lipid chain order parameter is the average over the two chains of the same lipids in the entire bilayer and certain simulation periods.

Voronoi tessellation analysis. In this work, Voronoi analysis was used to quantify the detailed local packing disruption of the lipid membrane by the NP. The lipid DPPC/DUPC COM is used for Voronoi tessellation analysis, which divided the lipid bilayer plane into polygonal regions based on the vertical bisector of two adjacent lipids, and each polygonal region represented the area of a single lipid. For clarity, the area per lipid was directly colored with the area value for visualization. These processes were implemented using MATLAB.

Membrane thickness. The membrane thickness was calculated to investigate the effect of NPs' ligand rigidity on the membrane. A 16 × 16 grid on the plane was generated, and the information for every point of the grids was calculated; then MATLAB was used to reconstruct the calculated information. Moreover, in order to reduce edge effects, periodic boundary conditions and interpolation fitting were applied.

Umbrella sampling simulations

In order to reveal the penetration thermodynamics of NPs with different surface ligand rigidities in lipid raft/non-raft membrane domains, umbrella sampling⁴⁹ simulations and the WHAM analysis method⁵⁸ were used here. The COM distance between the NP and model lipid bilayers along the membrane normal (z axis) was chosen as the reaction coordinate (ξ) for umbrella sampling simulations. One raft-like lipid bilayer consisting of DPPC and CHOL in a molar ratio of 5 : 2, and one non-raft lipid bilayer containing only the unsaturated lipid DUPC were studied. In both cases, ξ ranges from 0 to 5 nm with $\Delta\xi = 0.2$ nm, resulting in 26 independent sampling windows. The starting configuration for each window was generated from a pull simulation, where the embedded NP was pulled away from the lipid bilayer. Harmonic potentials with a force constant of 1500 kJ mol⁻¹ nm⁻² were used to constrain the COM distance between the NP and the lipid membrane in the umbrella sampling simulations. Each umbrella window was run for 500 ns. The initial 100 ns was reserved for the equilibration process, while the last 400 ns of each 500 ns trajectory was used to calculate the potential of mean force (PMF, relative free energy) profiles. This 400 ns trajectory was evenly divided into four blocks. Block averaging was performed to obtain the mean value and standard deviation (s.d.).

Results and discussion

Effects of ligand rigidity on the partitioning dynamics of NPs in phase-separated lipid membranes

As indicated in our previous work,²¹ more hydrophobic NPs (C1 type in MARTINI force field⁴⁷) with sufficient surface coating have the tendency to partition into the lipid raft membrane domain. However, the exact localization of these NPs is

always very close to the interface between lipid raft and non-raft membrane domains. On the other hand, the modification density of 66% is much closer to the experimental situation.^{59,60} Hence, in the current work, we chose ultra-small hydrophobic ligand-modified NPs with C1 type beads for ligands and a modification density of 66% (details can be found in the Model and methods section). The maximum size of these NPs was still in the favorable NP size range to be encapsulated in the hydrophobic region of the lipid membrane.²⁰ Ligands with different stiffnesses were achieved by adopting weaker (70 kJ mol^{-1}) and stronger (700 kJ mol^{-1}) bond angle constraints. In our simulations, these NPs with different surface ligand rigidities were initially embedded in a randomly distributed three-component lipid bilayer containing DPPC/DUPC/CHOL (5:3:2). For each system, 5 μs CGMD simulation was performed. During the first 1 μs CGMD simulation, stable phase separation occurred forming the lipid raft and non-raft domains, which is consistent with previous research studies.^{21,28,61,62} We could clearly find that the raft domain is mainly composed of saturated lipids (DPPC and CHOL), while the main component of the lipid non-raft domain is unsaturated lipids (DUPC).

As shown in Fig. 2a and b, both the system snapshots and the 2D number-density map of DPPC molecules plus the relative location of the NP clearly indicated that rigid-NPs tended to reside in the bulk raft domain, while soft-NPs preferentially

selected the boundary of the non-raft domain and the lipid raft domain. It is further quantitatively validated in Fig. 2c that the raft affinity of the ligand-modified NP could be improved by increasing the ligand rigidity. This role of surface ligand rigidity in NP's raft affinity shares the same mechanism with the role of ligand modification density,²¹ where 100% ligand modification (C1 type) and longer ligands can fully encapsulate the NP core to make the external molecules only sense the presence of surface ligands. Similarly, in the case of soft NPs in the current work, the ligands are very flexible and can collapse onto the surface of the NP core, which even exposes part of the NP core, which prefers to interact with non-raft domain lipids. This explains why soft NPs prefer to locate around the boundary of the lipid raft domain. As for the rigid NPs, ligands almost do not collapse, which can well shield the presence of the NP core. Then, the hydrophobic ligands (C1 type) will bring NPs to the bulk raft domain. In short, the ligand rigidity affects the NP's raft affinity by tuning the conformation of the modified ligands and thus the interactions between the NP core and the surrounding lipids. Rigid ligands have a thicker modification thickness and thus induce weak interactions, which in turn makes the ligand hydrophobicity the dominant factor for NP's raft affinity. In real applications, the rigidity of molecules can be changed by varying the molecular packing (different physical interactions)⁵⁴ or chemical crosslinking (different chemical interactions)⁶³ with different external stimuli. Our results will provide helpful insights into the design of ligand-modified NPs with the stimuli-adaptive affinity for lipid rafts.

It is worth noting that there are always a few DUPC lipids covering the upper and lower parts of NPs when they penetrate into raft domains (Fig. 2a and e). On the other hand, NPs with higher raft affinity will have fewer DUPC lipids around (Fig. 2e). The presence of DUPC lipids accompanying NPs can be ascribed to the much more flexible lipid tail of unsaturated DUPC lipids, which makes them relatively easier to reside in the local curved area where NPs are embedded. On the other hand, the coverage of DUPC molecules on the NP surface can avoid direct contact between water molecules and the hydrophobic ligands, which are energy unfavorable. Moreover, the interdigitation between NP surface ligands and lipid chains brings spatial restrictions and additional entropy to these surrounding lipids in both the membrane leaflets.^{64,65} Besides, NPs with a lower raft affinity tended to partition around the interface between the lipid raft and non-raft domains, which gave them more chances to directly interact with DUPC lipids (Fig. 2e). In other words, an NP with higher raft affinity has more contacts with the raft domain lipids (*e.g.* DPPC, Fig. 2d).

The designed ultra-small hydrophobic NPs first need to enter into the hydrophobic region of the lipid membrane and then partition into their preferred localization. As for the latter, our above results indicate that the surface ligand rigidity can regulate the raft affinity of ultra-small hydrophobic NPs. In order to evaluate how the ligand rigidity affects NP's translocation ability to enter into the lipid membrane, we performed umbrella sampling simulations and WHAM analysis to obtain

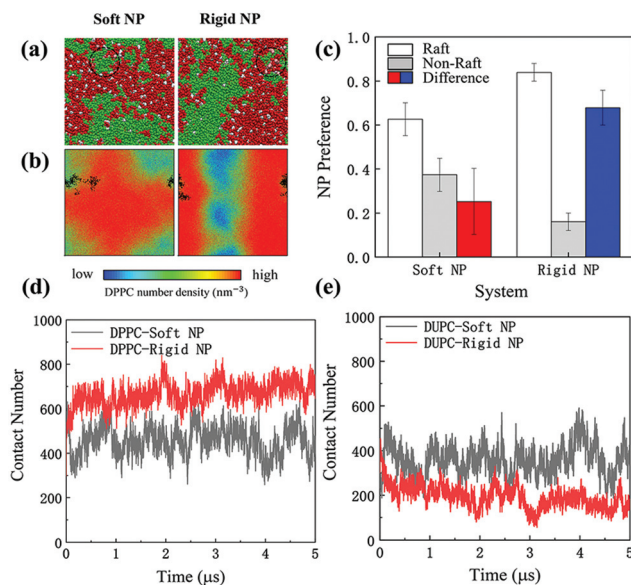


Fig. 2 Effects of ligand rigidity on the membrane partitioning dynamics of ligand-modified NPs. (a) Top-view system snapshots of the last frame of each 5 μs trajectory. Dashed black circles indicate the localization of NPs. (b) 2D number-density maps of DPPC molecules and the instantaneous location of NPs (black points) derived from analysis over the last 1 μs trajectory. (c) Percentage contact of NPs with raft domain lipids, non-raft domain lipids, and their differences for NP-embedded lipid membrane systems. Time evolution of contact number of NPs with (d) DPPC and (e) DUPC. The coloring style is the same as in Fig. 1.

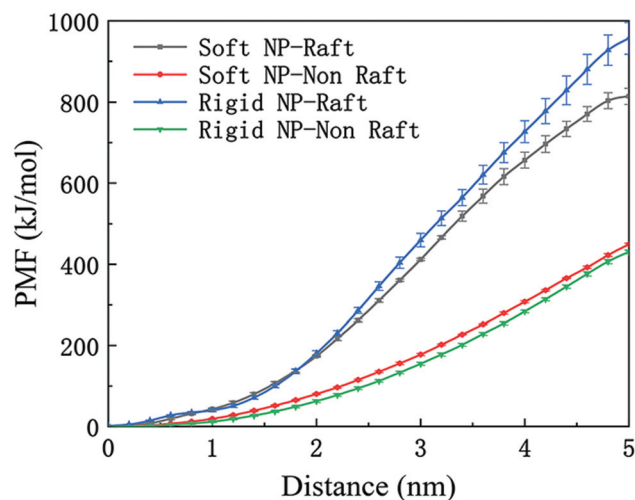


Fig. 3 PMF profiles for NP translocating into raft/non-raft membrane domains. Error bars are standard deviations based on the statistics from four 100 ns blocks over the last 400 ns of 500 ns trajectories.

the PMF profiles for NPs translocating into raft/non-raft membrane domains. When small molecules/NPs begin to induce disruption to the nearby lipids and spontaneously enter into the lipid membrane,^{66–70} there is usually an affordable energy barrier at the lipid head-group region where the resistance force is slightly greater than the driving force. The resistance force is mainly due to the steric hindrance. In our cases, no net energy barriers exist (Fig. 3). This is probably due to the strong hydrophobicity of NPs, which gives NPs a strong penetration ability and an overwhelming advantage over the translocation barrier.⁷¹ As shown in Fig. 3, both soft and rigid NPs (C1-type ligands) showed much more preferred localization in the hydrophobic region of the raft-like lipid bilayer than that of the non-raft-like lipid bilayer. Compared to soft NPs, the penetration ability of rigid NPs into the raft-like lipid bilayer is better. In other words, the surface ligand rigidity can affect the lipid raft targeting efficiency of these ultra-small hydrophobic NPs, and the membrane partitioning dynamics (raft affinity) after they enter into the lipid membrane.

Embedded NPs show no significant effects on the properties of phase-separated lipid membranes

To evaluate the effects of embedded NPs on the general properties of phase-separated lipid bilayers (DPPC/DUPC/CHOL), we analyzed the normalized lateral contacts of unsaturated lipids (Fig. S1†), lipid chain order parameters (Fig. S2†), cholesterol preferences (Fig. S3†) and lipid diffusion coefficients (Fig. S4 and Table S1†), which are essential indicators for the lipid raft dynamics.^{28,72} The results clearly showed that the embedded NPs in our work did not have significant effects on the lipid raft dynamics. In other words, NPs of this kind will be suitable for targeting raft or non-raft domains without significantly disrupting the properties of the overall membrane domains. In order to further evaluate the NPs' local disturb-

ance to the membrane region around the NP, we used a 2D phase map that provides the location of each lipid and its corresponding chain order parameters (Fig. 4 and Fig. S5†). As shown in the map, the lipid chain order differences between saturated (DPPC) and unsaturated (DUPC) lipids became more obvious when the lipid bilayer was fully phase-separated (Fig. 4 and Fig. S6†). Moreover, for the case of rigid NPs (Fig. 4), both in the upper and lower layers of the lipid membrane, chain order parameters of the closely surrounding lipids became smaller than other saturated lipids far from the NP, indicating that the encapsulation of the NP could induce the local membrane curvature and make the surrounding molecules disordered. As for soft NPs (Fig. S5†), their disturbance to the surrounding lipids was less obvious compared to rigid NPs.

In addition to the lipid chain order parameters, the effects of the embedded NPs on the local membrane packing and thickness were also quantified. The COM positions of lipids were used for 2D Voronoi tessellation analysis in the x - y plane. As shown in Fig. 5b, in each Voronoi polygon, the point is the COM position of the corresponding lipid. The area of the polygon represents the area of the corresponding lipid, which is visualized according to its value. We found that rigid NPs greatly increased the area occupied by the surrounding lipids after they embedded themselves into the raft domain, while soft NPs seldom disrupted the local membrane packing. The reason for this can be ascribed to the size^{11,73,74} and flexibility of NPs.^{66,75,76} Soft NPs, which have small flexible ligand mole-

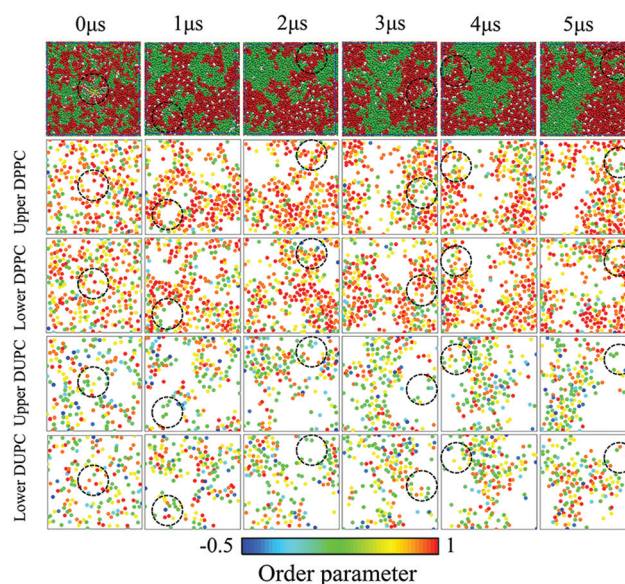


Fig. 4 Time evolution of system snapshots and lipid order parameters for each lipid of NP-embedded lipid membrane systems (ligand rigidity: rigid, ligand density: 66%). Each point represents one DPPC/DUPC molecule, and its color shows the averaged chain order parameters over the two lipid chains. The dashed black circle indicates the localization of the ligand-modified NP. The coloring style of system snapshots is the same as in Fig. 1.

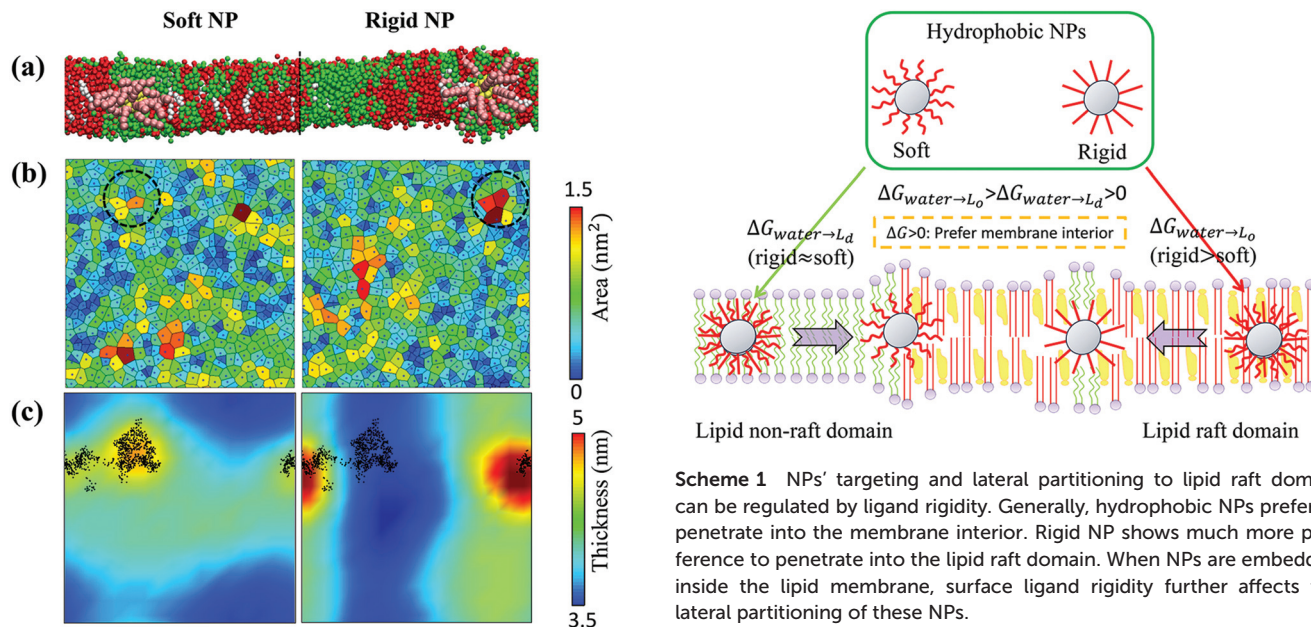


Fig. 5 Encapsulation of NPs with different ligand rigidities affects the local membrane structure differently. (a) Side-view system snapshots of the last frame of each 5 μs trajectory. (b) 2D Voronoi tessellation analysis of lipids in one monolayer in the x - y plane at the end of 5 μs trajectory. Dots denote the center-of-mass of the DPPC/DUPC/CHOL molecules. (c) Local membrane thickness distribution for simulation systems averaged over the last 1 μs . The black point corresponds to the NP's trajectory projected in the x - y plane. The coloring style is the same as in Fig. 1.

cules tend to collapse on the surface of the NP core during the simulation process, so the volume of the entire NPs will be much smaller than that of rigid NPs. In addition, when NPs enter the phospholipid membrane, softer ligands can change their conformations accordingly and thus have less impact on the lipid bilayers. In contrast, rigid NPs with stiffer ligands can insert into the lipid bilayer easily, which may cause much greater disruptions to the surrounding lipids. The effects of these NPs on the local membrane packing (Fig. 5) and lipid chain order parameters (Fig. 4) mentioned above are consistent. Besides, in both cases, the embedding of NPs did not significantly change the overall thickness of the raft or non-raft membrane domain. However, they indeed greatly increased the local membrane thickness or membrane curvature, and the effect of rigid NPs on the local membrane thickness was much more obvious. Similarly, rigid ligands increased the effective size of the ligand-modified NPs. The size differences of these NPs directly caused different effects on the local membrane thickness.^{21,60}

Conclusions

In this work, we investigated the role of surface ligand rigidity in determining the membrane partition kinetics of hydrophobic ligand-modified NPs (C1-type ligands). By changing the

force constants of the bond angle constraints within surface ligands, we obtained model hydrophobic NPs of different surface ligand rigidities without changing the chemical properties (e.g. hydrophobicity) of ligands. This makes surface ligand rigidity the only variable in our study. Through μs -scale CGMD simulations, our results clearly indicated that the preferred localization of hydrophobic NPs could be modulated by the surface ligand rigidity. Rigid NPs tend to locate into the bulk region of the lipid raft domain, while soft NPs prefer the lipid raft domain boundary. On the other hand, PMF profiles obtained from umbrella sampling simulations showed that the hydrophobic NPs preferred to penetrate into the lipid raft domain, and ligand rigidity could affect the corresponding penetration ability. In other words, the ligand rigidity could regulate both the targeting ability and affinity of hydrophobic NPs to the lipid raft domain (Scheme 1). Besides, our results further demonstrated that these NPs did not have significant effects on the overall properties of membrane domains, except for the local disturbance. All these data elucidated the essential role of surface ligand rigidity in lipid raft targeting ability and affinity, which could provide useful insights into the design of suitable nanoprobes to target the lipid raft domain and regulate the corresponding protein-lipid interactions.

Author contributions

Conceptualization: X.B.L.; Methodology: X.B.L. and X.Q.L.; Formal analysis: X.Q.L. and X.B.L.; Investigation and visualization: X.Q.L. and X.B.L.; Writing-original draft: X.Q.L.; Writing-review and editing: X.B.L.; Funding acquisition: X.B.L.; Project administration: X.B.L. All authors have read and agreed to the published version of the manuscript.

Conflicts of interest

The authors declare no competing interests.

Acknowledgements

This work was supported by the National Natural Science Foundation of China (No. 21903002), the Fundamental Research Funds for the Central Universities (No. YWF-20-BJ-J-632), and the Open Fund of State Key Laboratory of Membrane Biology (No. 2020KF09). We are grateful to the Center for High Performance Computing of Beihang University (BHHPC) for its generous computing resources.

References

- 1 D. Kim, J. Kim, Y. I. Park, N. Lee and T. Hyeon, Recent Development of Inorganic Nanoparticles for Biomedical Imaging, *ACS Cent. Sci.*, 2018, **4**, 324–336.
- 2 R. Kotcherlakota, S. Nimushakavi, A. Roy, H. C. Yadavalli, S. Mukherjee, S. Haque and C. R. Patra, Biosynthesized Gold Nanoparticles: In Vivo Study of near-Infrared Fluorescence (Nir)-Based Bio-Imaging and Cell Labeling Applications, *ACS Biomater. Sci. Eng.*, 2019, **5**, 5439–5452.
- 3 J. K. Awino, S. Gudipati, A. K. Hartmann, J. J. Santiana, D. F. Cairns-Gibson, N. Gomez and J. L. Rouge, Nucleic Acid Nanocapsules for Enzyme-Triggered Drug Release, *J. Am. Chem. Soc.*, 2017, **139**, 6278–6281.
- 4 S. H. Lee, O. K. Park, J. Kim, K. Shin, C. G. Pack, K. Kim, G. Ko, N. Lee, S.-H. Kwon and T. Hyeon, Deep Tumor Penetration of Drug-Loaded Nanoparticles by Click Reaction-Assisted Immune Cell Targeting Strategy, *J. Am. Chem. Soc.*, 2019, **141**, 13829–13840.
- 5 Y. Lin, J. Liu, R. Bai, J. Shi, X. Zhu, J. Liu, J. Guo, W. Zhang, H. Liu and Z. Liu, Mitochondria-Inspired Nanoparticles with Microenvironment-Adapting Capacities for on-Demand Drug Delivery after Ischemic Injury, *ACS Nano*, 2020, **14**, 11846–11859.
- 6 C.-C. Chang, T. K. Dinh, Y.-A. Lee, F.-N. Wang, Y.-C. Sung, P.-L. Yu, S.-C. Chiu, Y.-C. Shih, C.-Y. Wu and Y.-D. Huang, Nanoparticle Delivery of MnO_2 and Antiangiogenic Therapy to Overcome Hypoxia-Driven Tumor Escape and Suppress Hepatocellular Carcinoma, *ACS Appl. Mater. Interfaces*, 2020, **12**, 44407–44419.
- 7 D. Luo, X. Wang, E. Walker, J. Wang, S. Springer, J. Lou, G. Ramamurthy, C. Burda and J. P. Babilion, Nanoparticles Yield Increased Drug Uptake and Therapeutic Efficacy Upon Sequential near-Infrared Irradiation, *ACS Nano*, 2020, **14**, 15193–15203.
- 8 H. Geng, G. Poologasundarampillai, N. Todd, A. Devlin-Mullin, K. L. Moore, Z. Golrokhi, J. B. Gilchrist, E. Jones, R. J. Potter and C. Sutcliffe, Biotransformation of Silver Released from Nanoparticle Coated Titanium Implants Revealed in Regenerating Bone, *ACS Appl. Mater. Interfaces*, 2017, **9**, 21169–21180.
- 9 L. Wang, N. Hartel, K. Ren, N. A. Graham and N. Malmstadt, Effect of Protein Corona on Nanoparticle–Plasma Membrane and Nanoparticle–Biomimetic Membrane Interactions, *Environ. Sci.: Nano*, 2020, **7**, 963–974.
- 10 A. G. Rodríguez-Hernández, R. Vazquez-Duhalt and A. Huerta-Saquero, Nanoparticle-Plasma Membrane Interactions: Thermodynamics, Toxicity and Cellular Response, *Curr. Med. Chem.*, 2020, **27**, 3330–3345.
- 11 X. Lin, Y. Li and N. Gu, Nanoparticle's Size Effect on Its Translocation across a Lipid Bilayer: A Molecular Dynamics Simulation, *J. Comput. Theor. Nanosci.*, 2010, **7**, 269–276.
- 12 C. D. Walkey, J. B. Olsen, H. Guo, A. Emili and W. C. Chan, Nanoparticle Size and Surface Chemistry Determine Serum Protein Adsorption and Macrophage Uptake, *J. Am. Chem. Soc.*, 2012, **134**, 2139–2147.
- 13 X. Lin, Y. Y. Zuo and N. Gu, Shape Affects the Interactions of Nanoparticles with Pulmonary Surfactant, *Sci. China Mater.*, 2015, **58**, 28–37.
- 14 W. Wang, K. Gaus, R. D. Tilley and J. J. Gooding, The Impact of Nanoparticle Shape on Cellular Internalisation and Transport: What Do the Different Analysis Methods Tell Us?, *Mater. Horiz.*, 2019, **6**, 1538–1547.
- 15 X. Bai, S. Wang, X. Yan, H. Zhou, J. Zhan, S. Liu, V. K. Sharma, G. Jiang, H. Zhu and B. Yan, Regulation of Cell Uptake and Cytotoxicity by Nanoparticle Core under the Controlled Shape, Size, and Surface Chemistries, *ACS Nano*, 2019, **14**, 289–302.
- 16 P. Hu, W. Qian, B. Liu, C. Pichan and Z. Chen, Molecular Interactions between Gold Nanoparticles and Model Cell Membranes: A Study of Nanoparticle Surface Charge Effect, *J. Phys. Chem. C*, 2016, **120**, 22718–22729.
- 17 E. Heikkilä, H. Martínez-Seara, A. A. Gurtovenko, M. Javanainen, H. Häkkinen, I. Vattulainen and J. Akola, Cationic Au Nanoparticle Binding with Plasma Membrane-Like Lipid Bilayers: Potential Mechanism for Spontaneous Permeation to Cells Revealed by Atomistic Simulations, *J. Phys. Chem. C*, 2014, **118**, 11131–11141.
- 18 R. C. Van Lehn, P. U. Atukorale, R. P. Carney, Y.-S. Yang, F. Stellacci, D. J. Irvine and A. Alexander-Katz, Effect of Particle Diameter and Surface Composition on the Spontaneous Fusion of Monolayer-Protected Gold Nanoparticles with Lipid Bilayers, *Nano Lett.*, 2013, **13**, 4060–4067.
- 19 J. Wang, W. Li and J. Zhu, Encapsulation of Inorganic Nanoparticles into Block Copolymer Micellar Aggregates: Strategies and Precise Localization of Nanoparticles, *Polymer*, 2014, **55**, 1079–1096.
- 20 X. Chen, D. P. Tieleman and Q. Liang, Modulating Interactions between Ligand-Coated Nanoparticles and Phase-Separated Lipid Bilayers by Varying the Ligand Density and the Surface Charge, *Nanoscale*, 2018, **10**, 2481–2491.

- 21 X. Lin, X. Lin and N. Gu, Optimization of Hydrophobic Nanoparticles to Better Target Lipid Rafts with Molecular Dynamics Simulations, *Nanoscale*, 2020, **12**, 4101–4109.
- 22 J. Liang, P. Chen, B. Dong, Z. Huang, K. Zhao and L.-T. Yan, Ligand–Receptor Interaction-Mediated Transmembrane Transport of Dendrimer-Like Soft Nanoparticles: Mechanisms and Complicated Diffusive Dynamics, *Biomacromolecules*, 2016, **17**, 1834–1844.
- 23 L. Zhang, H. Chen, J. Xie, M. Becton and X. Wang, Interplay of Nanoparticle Rigidity and Its Translocation Ability through Cell Membrane, *J. Phys. Chem. B*, 2019, **123**, 8923–8930.
- 24 R. C. Van Lehn and A. Alexander-Katz, Fusion of Ligand-Coated Nanoparticles with Lipid Bilayers: Effect of Ligand Flexibility, *J. Phys. Chem. A*, 2014, **118**, 5848–5856.
- 25 H.-m. Ding and Y.-q. Ma, Role of Physicochemical Properties of Coating Ligands in Receptor-Mediated Endocytosis of Nanoparticles, *Biomaterials*, 2012, **33**, 5798–5802.
- 26 K. Simons and D. Toomre, Lipid Rafts and Signal Transduction, *Nat. Rev. Mol. Cell Biol.*, 2000, **1**, 31–39.
- 27 E. Sezgin, I. Levental, S. Mayor and C. Eggeling, The Mystery of Membrane Organization: Composition, Regulation and Roles of Lipid Rafts, *Nat. Rev. Mol. Cell Biol.*, 2017, **18**, 361.
- 28 X. Lin, J. H. Lorent, A. D. Skinkle, K. R. Levental, M. N. Waxham, A. A. Gorfe and I. Levental, Domain Stability in Biomimetic Membranes Driven by Lipid Polyunsaturation, *J. Phys. Chem. B*, 2016, **120**, 11930–11941.
- 29 P. W. Fowler, J. J. Williamson, M. S. Sansom and P. D. Olmsted, Roles of Interleaflet Coupling and Hydrophobic Mismatch in Lipid Membrane Phase-Separation Kinetics, *J. Am. Chem. Soc.*, 2016, **138**, 11633–11642.
- 30 X. Lin, Z. Li and A. A. Gorfe, Reversible Effects of Peptide Concentration and Lipid Composition on H-Ras Lipid Anchor Clustering, *Biophys. J.*, 2015, **109**, 2467–2470.
- 31 S. Zhang and X. Lin, Lipid Acyl Chain Cis Double Bond Position Modulates Membrane Domain Registration/Anti-Registration, *J. Am. Chem. Soc.*, 2019, **141**, 15884–15890.
- 32 X. Lin, S. Zhang, H. Ding, I. Levental and A. A. Gorfe, The Aliphatic Chain of Cholesterol Modulates Bilayer Interleaflet Coupling and Domain Registration, *FEBS Lett.*, 2016, **590**, 3368–3374.
- 33 J. D. Nickels, J. C. Smith and X. Cheng, Lateral Organization, Bilayer Asymmetry, and, Inter-Leaflet Coupling of Biological Membranes, *Chem. Phys. Lipids*, 2015, **192**, 87–99.
- 34 S. Y. Lee, S.-H. Ko, J.-S. Shim, D.-D. Kim and H.-J. Cho, Tumor Targeting and Lipid Rafts Disrupting Hyaluronic Acid-Cyclodextrin-Based Nanoassembled Structure for Cancer Therapy, *ACS Appl. Mater. Interfaces*, 2018, **10**, 36628–36640.
- 35 D. Yurtsever and J. H. Lorent, Structural Modifications Controlling Membrane Raft Partitioning and Curvature in Human and Viral Proteins, *J. Phys. Chem. B*, 2020, **124**, 7574–7585.
- 36 C. J. Newcomb, S. Sur, S. S. Lee, J. M. Yu, Y. Zhou, M. L. Snead and S. I. Stupp, Supramolecular Nanofibers Enhance Growth Factor Signaling by Increasing Lipid Raft Mobility, *Nano Lett.*, 2016, **16**, 3042–3050.
- 37 A. D. Shah, K. L. Inder, A. K. Shah, A. S. Cristino, A. B. McKie, H. Gabra, M. J. Davis and M. M. Hill, Integrative Analysis of Subcellular Quantitative Proteomics Studies Reveals Functional Cytoskeleton Membrane–Lipid Raft Interactions in Cancer, *J. Proteome Res.*, 2016, **15**, 3451–3462.
- 38 P. Panja and N. R. Jana, Lipid-Raft-Mediated Direct Cytosolic Delivery of Polymer-Coated Soft Nanoparticles, *J. Phys. Chem. B*, 2020, **124**, 5323–5333.
- 39 J. Lin, H. Zhang, Z. Chen and Y. Zheng, Penetration of Lipid Membranes by Gold Nanoparticles: Insights into Cellular Uptake, Cytotoxicity, and Their Relationship, *ACS Nano*, 2010, **4**, 5421–5429.
- 40 X. Quan, C. Peng, D. Zhao, L. Li, J. Fan and J. Zhou, Molecular Understanding of the Penetration of Functionalized Gold Nanoparticles into Asymmetric Membranes, *Langmuir*, 2017, **33**, 361–371.
- 41 T. Lunnoo, J. Assawakhajornsak, S. Ruangchai and T. Puangmali, Role of Surface Functionalization on Cellular Uptake of Aunps Characterized by Computational Microscopy, *J. Phys. Chem. B*, 2020, **124**, 1898–1908.
- 42 P. Patel, K. P. Santo, S. Burgess, A. Vishnyakov and A. V. Neimark, Stability of Lipid Coatings on Nanoparticle-Decorated Surfaces, *ACS Nano*, 2020, **14**, 17273–17284.
- 43 T. Lunnoo, J. Assawakhajornsak and T. Puangmali, In Silico Study of Gold Nanoparticle Uptake into a Mammalian Cell: Interplay of Size, Shape, Surface Charge, and Aggregation, *J. Phys. Chem. C*, 2019, **123**, 3801–3810.
- 44 W. Noid, J.-W. Chu, G. S. Ayton, V. Krishna, S. Izvekov, G. A. Voth, A. Das and H. C. Andersen, The Multiscale Coarse-Graining Method. I. A Rigorous Bridge between Atomistic and Coarse-Grained Models, *J. Chem. Phys.*, 2008, **128**, 244114.
- 45 G. S. Ayton and G. A. Voth, Hybrid Coarse-Graining Approach for Lipid Bilayers at Large Length and Time Scales, *J. Phys. Chem. B*, 2009, **113**, 4413–4424.
- 46 T. S. Carpenter, C. A. López, C. Neale, C. Montour, H. I. Ingólfsson, F. Di Natale, F. C. Lightstone and S. Gnanakaran, Capturing Phase Behavior of Ternary Lipid Mixtures with a Refined Martini Coarse-Grained Force Field, *J. Chem. Theory Comput.*, 2018, **14**, 6050–6062.
- 47 S. J. Marrink, H. J. Risselada, S. Yefimov, D. P. Tieleman and A. H. De Vries, The Martini Force Field: Coarse Grained Model for Biomolecular Simulations, *J. Phys. Chem. B*, 2007, **111**, 7812–7824.
- 48 H.-Y. Lee, S. H. R. Shin, L. L. Abezgauz, S. A. Lewis, A. M. Chirsan, D. D. Danino and K. J. M. Bishop, Integration of Gold Nanoparticles into Bilayer Structures Via Adaptive Surface Chemistry, *J. Am. Chem. Soc.*, 2013, **135**, 5950–5953.

- 49 G. M. Torrie and J. P. Valleau, Nonphysical Sampling Distributions in Monte Carlo Free-Energy Estimation: Umbrella Sampling, *J. Comput. Phys.*, 1977, **23**, 187–199.
- 50 S. Pronk, S. Páll, R. Schulz, P. Larsson, P. Bjelkmar, R. Apostolov, M. R. Shirts, J. C. Smith, P. M. Kasson and D. van der Spoel, Gromacs 4.5: A High-Throughput and Highly Parallel Open Source Molecular Simulation Toolkit, *Bioinformatics*, 2013, **29**, 845–854.
- 51 G. Bussi, D. Donadio and M. Parrinello, Canonical Sampling through Velocity Rescaling, *J. Comput. Phys.*, 2007, **126**, 014101.
- 52 M. Parrinello and A. Rahman, Polymorphic Transitions in Single Crystals: A New Molecular Dynamics Method, *J. Appl. Phys.*, 1981, **52**, 7182–7190.
- 53 C.-T. Lai, W. Sun, R. U. Palekar, C. S. Thaxton and G. C. Schatz, Molecular Dynamics Simulation and Experimental Studies of Gold Nanoparticle Templated Hdl-Like Nanoparticles for Cholesterol Metabolism Therapeutics, *ACS Appl. Mater. Interfaces*, 2017, **9**, 1247–1254.
- 54 K. R. Raghupathi, U. Sridhar, K. Byrne, K. Raghupathi and S. Thayumanavan, Influence of Backbone Conformational Rigidity in Temperature-Sensitive Amphiphilic Supramolecular Assemblies, *J. Am. Chem. Soc.*, 2015, **137**, 5308–5311.
- 55 W. Humphrey, A. Dalke and K. Schulten, Vmd: Visual Molecular Dynamics, *J. Mol. Graphics*, 1996, **14**, 33–38.
- 56 T. A. Wassenaar, H. I. Ingólfsson, R. A. Böckmann, D. P. Tieleman and S. J. Marrink, Computational Lipidomics with Insane: A Versatile Tool for Generating Custom Membranes for Molecular Simulations, *J. Chem. Theory Comput.*, 2015, **11**, 2144–2155.
- 57 S. J. Marrink and D. P. Tieleman, Perspective on the Martini Model, *Chem. Soc. Rev.*, 2013, **42**, 6801–6822.
- 58 S. Kumar, J. M. Rosenberg, D. Bouzida, R. H. Swendsen and P. A. Kollman, The Weighted Histogram Analysis Method for Free-Energy Calculations on Biomolecules. I. The Method, *J. Comput. Chem.*, 1992, **13**, 1011–1021.
- 59 H. Liu, H.-Y. Zhao, F. Müller-Plathe, H.-J. Qian, Z.-Y. Sun and Z.-Y. Lu, Distribution of the Number of Polymer Chains Grafted on Nanoparticles Fabricated by Grafting-to and Grafting-from Procedures, *Macromolecules*, 2018, **51**, 3758–3766.
- 60 R. Shi, H.-J. Qian and Z.-Y. Lu, Tuning Cavitation and Crazing in Polymer Nanocomposite Glasses Containing Bimodal Grafted Nanoparticles at the Nanoparticle/Polymer Interface, *Phys. Chem. Chem. Phys.*, 2019, **21**, 7115–7126.
- 61 I.-H. Lee, M. Y. Imanaka, E. H. Modahl and A. P. Torres-Ocampo, Lipid Raft Phase Modulation by Membrane-Anchored Proteins with Inherent Phase Separation Properties, *ACS Omega*, 2019, **4**, 6551–6559.
- 62 R. Dong, Y. Tan, A. Fan, Z. Liao, H. Liu and P. Wei, Molecular Dynamics of the Recruitment of Immunoreceptor Signaling Module Dap12 Homodimer to Lipid Raft Boundary Regulated by Pip2, *J. Phys. Chem. B*, 2019, **124**, 504–510.
- 63 N. G. Lemcoff, T. A. Spurlin, A. A. Gewirth, S. C. Zimmerman, J. B. Beil, S. L. Elmer and H. G. Vandever, Organic Nanoparticles Whose Size and Rigidity Are Finely Tuned by Cross-Linking the End Groups of Dendrimers, *J. Am. Chem. Soc.*, 2004, **126**, 11420–11421.
- 64 D. Hakobyan and A. Heuer, Key Molecular Requirements for Raft Formation in Lipid/Cholesterol Membranes, *PLoS One*, 2014, **9**, e87369.
- 65 S. Y. Noh, A. Nash and R. Notman, The Aggregation of Striped Nanoparticles in Mixed Phospholipid Bilayers, *Nanoscale*, 2020, **12**, 4868–4881.
- 66 S. Wang, H. Guo, Y. Li and X. Li, Penetration of Nanoparticles across a Lipid Bilayer: Effects of Particle Stiffness and Surface Hydrophobicity, *Nanoscale*, 2019, **11**, 4025–4034.
- 67 A. R. Zolghadr and S. S. Moosavi, Interactions of Neutral Gold Nanoparticles with Dppc and Popc Lipid Bilayers: Simulation and Experiment, *RSC Adv.*, 2019, **9**, 5197–5205.
- 68 D. Toroz, T. Khanna and I. R. Gould, Modeling the Effect of Bsep Inhibitors in Lipid Bilayers by Means of All-Atom Molecular Dynamics Simulation, *ACS Omega*, 2019, **4**, 3341–3350.
- 69 P. Gkeka, L. Sarkisov and P. Angelikopoulos, Homogeneous Hydrophobic–Hydrophilic Surface Patterns Enhance Permeation of Nanoparticles through Lipid Membranes, *J. Phys. Chem. Lett.*, 2013, **4**, 1907–1912.
- 70 R. C. Van Lehn and A. Alexander-Katz, Energy Landscape for the Insertion of Amphiphilic Nanoparticles into Lipid Membranes: A Computational Study, *PLoS One*, 2019, **14**, e0209492.
- 71 R. Qiao, A. P. Roberts, A. S. Mount, S. J. Klaine and P. C. Ke, Translocation of C60 and Its Derivatives across a Lipid Bilayer, *Nano Lett.*, 2007, **7**, 614–619.
- 72 D. Marguet, P. F. Lenne, H. Rigneault and H. T. He, Dynamics in the Plasma Membrane: How to Combine Fluidity and Order, *EMBO J.*, 2006, **25**, 3446–3457.
- 73 B. Lu, T. Smith and J. J. Schmidt, Nanoparticle–Lipid Bilayer Interactions Studied with Lipid Bilayer Arrays, *Nanoscale*, 2015, **7**, 7858–7866.
- 74 B. Jing and Y. Zhu, Disruption of Supported Lipid Bilayers by Semihydrophobic Nanoparticles, *J. Am. Chem. Soc.*, 2011, **133**, 10983–10989.
- 75 J. Sun, L. Zhang, J. Wang, Q. Feng, D. Liu, Q. Yin, D. Xu, Y. Wei, B. Ding and X. Shi, Tunable Rigidity of (Polymeric Core)–(Lipid Shell) Nanoparticles for Regulated Cellular Uptake, *Adv. Mater.*, 2015, **27**, 1402–1407.
- 76 H. Deng, K. Song, J. Zhang, L. Deng, A. Dong and Z. Qin, Modulating the Rigidity of Nanoparticles for Tumor Penetration, *ChemComm*, 2018, **54**, 3014–3017.